




Heavy metal removal from industrial effluent using bio-sorbent blends

I. Sreedhar¹  · N. Saketharam Reddy¹

© Springer Nature Switzerland AG 2019

Abstract

There is extensive literature on the use of adsorbents derived from waste to treat industrial effluents containing heavy metal ions. However, there is limited information on the use of adsorbent blends. This is applicable for treating effluents which contain a number of heavy metals, so any one single adsorbent may not be suitable for achieving high percent removal of all ions. The present work employs adsorbent blends to treat an electrochemical effluent in batch mode. This work aims to provide valuable insights on the interaction of heavy metals with the adsorbents in blends. Effluent from an electrochemical industry was treated with blends of calcium bentonite, fly ash and wheat bran in different compositions to remove heavy metal ions (Fe, Ni, Cu, As, Zn, Cd) from an aqueous effluent solution. The optimal set of conditions identified were pH, 5–7; contact time, 60–90 min; agitation speed of 200 rpm; adsorbent dosage of 1 g/50 mL; and particle size of 150–300 μ . Metal ions arsenic, zinc and cadmium were completely removed. The percentage removal of (Fe, Ni, Cu) metal ions was in the order Fe(II)(96.73%) > Ni(II)(74.03%) > Cu(II)(70.70%) at optimum conditions in a short equilibrium time of 90 min. Batch experiments were conducted to determine the factors such as adsorbent composition, temperature, pH, agitation speed, dosage, contact time and particle size affecting adsorption, and all these parameters were found to strongly influence the adsorption. Experimental data were analyzed for Langmuir and Freundlich isotherms. Langmuir isotherm shows the maximum adsorption capacities were in order Fe(II) 146.1 mg/g > Ni(II) 115.9 mg/g > Cu(II) 74.5 mg/g. Freundlich parameter 'n' was found to be greater than 1 which showed that the adsorption is feasible for all three metals. Freundlich isotherm fit the data comparatively better, but neither of the two isotherms satisfactorily explained the adsorption, which indicated heterogeneity of adsorption. Kinetic studies were performed and analyzed for pseudo-first- and pseudo-second-order kinetics and the Weber–Morris intraparticle diffusion model. The adsorption data fit accurately to pseudo-second-order kinetic model with coefficient of correlation values greater than 0.99 for all three heavy metals. The kinetic constants were found to be 8.49×10^{-3} , 5.82×10^{-3} , $5.27 \times 10^{-3} \frac{\text{g}}{\text{mg min}}$ for Fe(II), Ni(II) and Cu(II), respectively. From the intraparticle diffusion model, it was inferred that there were different rate-limiting steps during the duration of the adsorption process, including intraparticle diffusion and boundary layer diffusion.

Keywords Heavy metal adsorption · Process standardization · Adsorption kinetics · Langmuir isotherm · Freundlich isotherm · Intraparticle diffusion · Batch reaction

1 Introduction

Water is one of the most essential elements for life on earth. But due to human activities, fresh water is getting polluted at an alarming rate. Rigorous studies were carried out all around the globe to study treatment of different

contaminants in industrial effluents. Heavy metals are one of the most toxic pollutants. Some well-known toxic metallic elements are arsenic, iron, chromium, cadmium, lead, nickel, copper, zinc and mercury. Heavy metals are toxic and non-biodegradable and can bio-accumulate in living cells [1]. Heavy metals not only damage human health

✉ I. Sreedhar, isreedhar2001@yahoo.co.in | ¹Department of Chemical Engineering, BITS Pilani Hyderabad Campus, Hyderabad, India.

SN Applied Sciences (2019) 1:1021 | <https://doi.org/10.1007/s42452-019-1057-4>

Received: 4 April 2019 / Accepted: 7 August 2019 / Published online: 12 August 2019

but also affect the environment and marine ecosystems and pose a significant health threat to aquatic life—most common being the damage of the gill of fish [2, 3]. Various methods to remove heavy metals exist such as chemical precipitation [4], membrane filtration [5], electrodialysis [6], photocatalysis [7], electrocoagulation [8] and adsorption [9]. Adsorption has been an important area of interest in the recent years, with majority latest research focused on identifying low-cost adsorbents [9]. Research work is also being done to synthesize new adsorbents with some recent advances in novel adsorbents which include using activated carbon synthesized from peanut shell [10], alizarin red-S-loaded amberlite IRA-400 anion exchange resin [11], starch/SnO₂ nanocomposite [12], Fe₃O₄ nanocomposites [13], MOF (metal organic framework)-based composites [14, 15], nickel ferrite bearing nitrogen-doped mesoporous carbon (NiFe₂O₄-NC) [16], nanocomposite cation exchanger sodium dodecyl sulfate acrylamide Zr(IV) selenite (SDS-AZS) [17] for removing toxic heavy metals. Such adsorbents are specially tailored to give them favorable properties like high adsorption capacity, regeneration capability, high surface area, mechanical and thermal stability [18, 19]. Currently, activated charcoal is the adsorbent of choice, but high costs are a concern [20]. Therefore, cheap bio-derived materials of renewable sources are suitable alternatives [21, 22]. Some of the common bio-adsorbents, bio-derived and industrial waste products used as adsorbents are bacteria [23], fungi [24], algae [25], tea waste [26], rice bran [27], egg shell [28], fuller's earth [29], fly ash [30] among others. The present study aims to use such low-cost adsorbents for treating a wide variety of heavy metals simultaneously. As we show in this work, these adsorbents are typically selective toward certain heavy metals and are not suitable for treating effluents with a number of different heavy metal ions. For such cases, it is proposed that a mixture of adsorbents be used to treat the effluent, so that all the ions may be removed. In this study, six adsorbents were used for initial screening, i.e., rice bran, wheat bran, sweet lime peel, egg shells, fly ash and Ca bentonite. At specified conditions, these adsorbents were employed to treat battery manufacturing effluent by batch adsorption. Among these adsorbents, three adsorbents, viz. wheat bran, fly ash and Ca bentonite, were selected based on their performance in the metal removal for further rigorous studies at the second level. Wheat bran is the shell of the wheat seed and is removed when processing wheat to flour [31]. Coal fly ash is an inorganic residue which is produced by combustion of coal and considered as an industrial waste and used as a filler in different applications [32, 33]. It has potential use in treating wastewater due to its chemical composition, i.e., silica, alumina, ferric oxide, magnesium oxide and calcium oxide, and its physical properties like surface area,

particle size and porosity [34]. Ca bentonite is clay which is in abundance in earth's crust. In the present study, investigations were conducted in three phases—initial screening of adsorbents from six suitable candidates, rigorous standardization and characterization (FTIR and BET) studies using selected sorbents and their blends vis-à-vis various critical process parameters like sorbent composition, contact time, dosage, agitation speed, particle size, pH and temperature to identify the optimal set of parameters to maximize the metal removal from the effluent and then finally fitting the experimental data to various adsorption isotherms like Langmuir and Freundlich and then estimating the kinetic parameters like reaction order, rate constant by proposing various kinetic models and fitting the experimental data to each to find the most suitable model. The role of intraparticle diffusion on the adsorption kinetics was studied by fitting the kinetic data to the Weber and Morris model. Thermodynamic parameters relating to adsorption of heavy metals were also calculated. It should be mentioned here that adsorbent blends are different from adsorbent composites. The adsorbent 'blending' in this work refers to simple mixing of the adsorbents in required weight ratio, while adsorbent 'composites' are made with the intent to improve the physical properties (thermal, mechanical, etc.) of the component adsorbents. Preparing these composites typically involve chemical reactions like cross-linking and surface treatment [35].

2 Materials and method

2.1 Materials

Materials used for the experiments are of analytical grades. Effluent was obtained from an electrochemical industry, and the adsorbent used for the experiments is sweet lime peel, egg shells, wheat bran, rice bran, fly ash and calcium bentonite. All the adsorbents were procured locally from Hyderabad. Chemicals used were sodium carbonate, sodium hydroxide, hydrochloric acid as buffer for pH adjustments. The effluent was analyzed using XRF, and the composition is given in Table 1. It had a pH of 0.4, TDS of 0 and turbidity of 0.64.

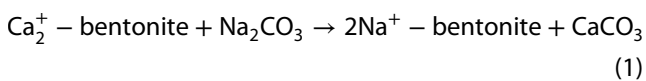
2.2 Adsorbent preparation

Sweet lime peel was washed several times with deionized water and dried first in sunlight and then in a hot oven at 90 °C till they became crisp. The dry peel was then ground into fine powder and sieved through a 425- μ sieve. This powder was washed with deionized double distilled water (DDDW) till the washings were color free. After this, the adsorbent was dried in an air oven at 105 °C till dry

Table 1 Effluent metal ion composition

Metal ion	Concentration (mg/L)
Fe(II)	931.8
Ni(II)	795.2
Cu(II)	578.3
Zn(II)	70.5
As(II)	4.9
Cd(II)	34.8

and crushed again [36]. Egg shells were washed with distilled water several times and then air-dried in a hot air oven at 40 °C for 30 min. They were then ground to powder [28]. Wheat bran was washed with DDDW water and then dried. After drying, wheat bran was ground to powder [31]. Rice bran was collected from a rice mill near Hyderabad. It was prepared for experiments after washing with DDDW water to remove dust and water-soluble impurities and then dried at 105 °C in an oven for 24 h and crushed to powder [27]. Sodium-activated bentonite was synthesized by treating Ca bentonite with 7.5% sodium carbonate according to Eq. (1). The settled clay was washed several times dried in an oven and stored in airtight bags [37]. Fly ash was dried at 110 °C for 2 h in an oven and stored in zip lock bags [30]. All the adsorbents were sieved to different fractions, viz. > 425, 425–300, 300–150, 150–75, < 75 μ, and stored in zip lock bags for ready use.



2.3 Experimental setup and procedure

2.3.1 Initial screening

Experiments were carried out with six different adsorbents, i.e., sweet lime peel, wheat bran, rice bran, fly ash, egg shells and Ca bentonite, in batch adsorption method. The experimental conditions used are listed in Table 2. The basis for choosing the best adsorbents is the percent removal of different metals from solution.

Table 2 Process conditions for adsorbents in the initial screening

Parameters (↓)/adsorbents (→)	Sweet lime	Egg shell	Wheat bran	Rice bran	Fly ash	Ca bentonite
pH	5	6	5	2	4	7
Temp (°C)	25	25	25	25	25	25
Agitation speed (rpm)	200	200	150	200	200	200
Dosage (g/100 mL)	0.2	1	2	2	2	0.5
Contact time (h)	3	1.5	1	1.5	1.5	1
Particle size (μ)	150–300	300–450	150–300	150–300	150–300	150–300

2.3.2 Characterization of adsorbents

The surface functional groups on the adsorbents were identified using Fourier transform infrared spectrometer Jasco FT/IR-4200 type A model in the wavenumber range of 4000–400 cm⁻¹ after preparing KBr pellets. The specific surface areas of the adsorbents were measured by BET method. The degassing temperature and time were 150 °C and 3 h, respectively, for all samples.

2.3.3 Adsorbent blends

To further enhance the metal removal efficiency, the three best adsorbents were used to make blends of different compositions CB–WB–FA as 33.3–33.3–33.3, 40–40–20, 20–20–60, 20–60–20, 20–40–40, 40–20–40, 60–20–20. Batch adsorption experiments were done with these blends with process conditions, viz. dosage as 1 g/50 ml solution, temperature of 30 °C, pH of 5.5, contact time 90 min, particle size 300–150 μ and 200 rpm agitation speed. The blend which gave maximum metal removal considering all metals was selected for further studies.

2.3.4 Process conditions to study effect of process parameters

Different process parameters, viz. contact time, pH, particle size, agitation speed, dosage and temperature, were considered for adsorption studies in metal removal. To study the effect of each of these parameters on adsorption, experiments were done with conditions listed in Table 3.

2.3.5 Estimation of adsorption capacity

The amount of metal ions adsorbed was calculated by the difference in initial and final concentration of metal ions. The percentage removal (%R) was calculated using the following equation:

$$\%R = \frac{C_0 - C_t}{C_0} \times 100 \quad (2)$$

Table 3 Process conditions used in experiments for each parameter studied

Parameters studied (↓) /process parameters (→)	Contact time (min)	pH	Particle size (μs)	Agitation speed (rpm)	Dosage (g/50 ml)	Temperature (°C)
Contact time	2,5,10,15,30,40,60,90,120	5.5	300–150	200	1	30
pH	90	2,3,8, 5.5, 7	300–150	200	1	30
Particle size	90	5.5	600–425,425–300, 300–150,150–75	200	1	30
Agitation speed	90	5.5	300–150	100,150,200,250	1	30
Dosage	90	5.5	300–150	200	0.2,0.5,0.7,1	30
Temperature	90	5.5	300–150	200	1	20,30,40,50

And the adsorption capacity (q_t) was calculated using Eq. 3.

$$q_t = \frac{(C_0 - C_t)V}{m} \tag{3}$$

where C_0 is the initial concentration of metal ion (mg/L), C_t is the concentration of metal ion at time t (mg/L), C_e is the concentration of metal ion at equilibrium (mg/L), m is the mass of adsorbent (g), V is the volume of solution (L) and q_t is the adsorption capacity at time t (mg/g).

3 Results and discussion

3.1 Initial screening

The adsorbents selected for initial screening, viz. sweet lime peel, egg shells, wheat bran, rice bran, fly ash and

calcium bentonite, were used in a batch adsorption method for the metal removal (Table 2). Figure 1 shows the performance analysis of these adsorbents in terms of percent removal of different metals from effluent. From the results, it is obvious that wheat bran (WB), fly ash (FA) and calcium bentonite (CB) exhibited better removal of heavy metals for most metals, and hence, these three adsorbents were chosen for making blends to achieve enhanced metal removal.

3.2 Adsorbent composition

To study the effect of adsorbent blend composition on percentage removal of different metal ions, experiments were done with specifications listed in Table 3. From the results that are depicted in Fig. 2 and Table 4, it is clear that the 33.33–33.33–33.33(CB–WB–FA) and the 60–20–20 blends are the best out of all studied blends. These two blends removed Zn, As, Cd completely after 90 min. The



Fig. 1 Percentage removal of metal ions using different adsorbents

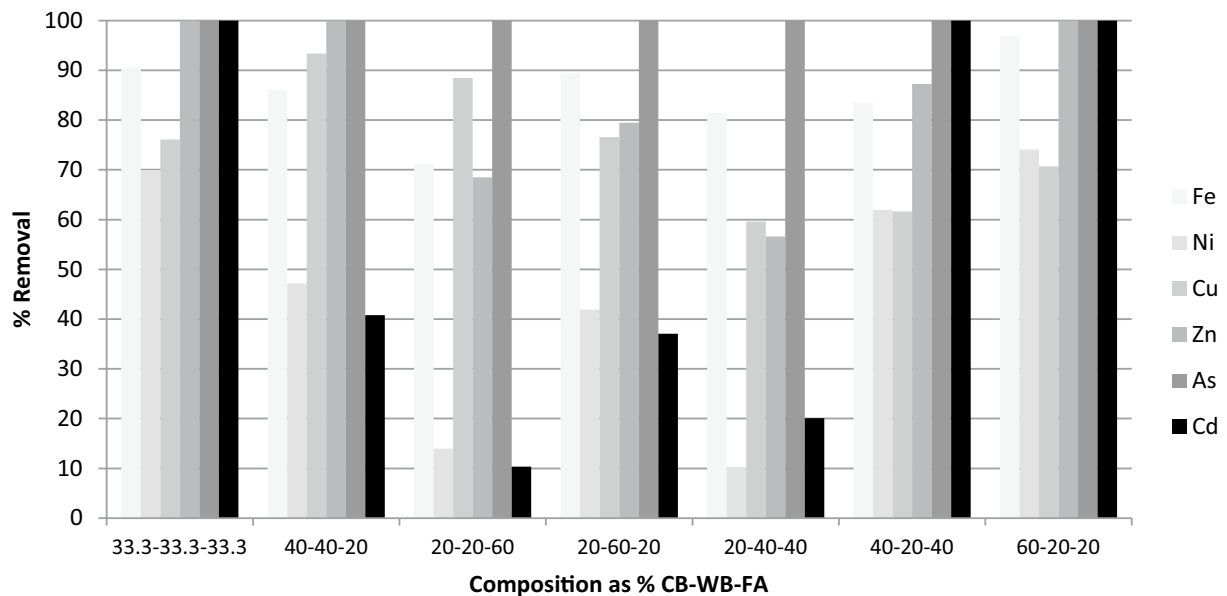


Fig. 2 Percentage removal of metal ions using different adsorbent blend compositions

Table 4 Percent removal of heavy metals using CB-WB-FA in different compositions at specified condition

Metals	33.3-33.3-33	40-40-20	20-20-60	20-60-20	20-40-40	40-20-40	60-20-20
Fe(II)	90.52	86.05	70.97	89.36	81.41	83.51	96.73
Ni(II)	69.96	47.14	13.94	41.87	10.31	61.9	74.03
Cu(II)	76.11	93.35	88.48	76.6	59.58	61.6	70.70
Zn(II)	100	100	68.51	79.43	56.59	87.23	100
As(II)	100	100	100	100	100	100	100
Cd(II)	100	40.80	10.34	37.06	20.11	100	100

former removed more Cu(II), while the latter removed more Fe(II) and Ni(II). Out of these two, 60-20-20 blend was chosen for further studies as it showed higher removal for Ni(II) and Fe(II) ions, which are more in concentration as compared to Cu(II), thus giving it a higher total adsorption capacity. The optimal results shown in Figs. 1 and 2 were reproduced with very good accuracy within an error of less than 4%.

3.3 Adsorbent characterization

The FTIR spectra of the three adsorbents CB, FA and WB are shown in Fig. 3a-c, respectively. In Fig. 3a, the calcium bentonite spectrum has peaks between 3200 and 3617 cm^{-1} which are attributed to stretching of lattice OH (Si-OH, Al-OH) and of the adsorbed water. The presence of silica $\text{O}=\text{Si}=\text{O}$ produces the peak at 1421.3 cm^{-1} . The overtone of bending vibration of water is seen at 1658.5 cm^{-1} . The deep band at 1026.9 cm^{-1} in the stretching mode region is because of $\text{Si}=\text{O}=\text{Si}$ stretching. Bands at 789.7 and 512 cm^{-1} in the stretching range

are because of Si-O-Al and Si-O-Mg stretching and Si-O bending frequencies [37]. In Fig. 3b, the spectra of fly ash are shown. The peak at 3438.5 cm^{-1} is due to -OH groups on the surface of fly ash and also due to the stretching vibrations of -OH in water molecules adsorbed on fly ash. The peak at 2923 cm^{-1} is due to C-H stretching vibration of organic carbon. Peak at 1636 cm^{-1} is due to aromatic C=C stretching of organic carbon. The peak at 1084 cm^{-1} is due to Si-O/Al-O stretching vibration, while 459 cm^{-1} is due to them in plane bending vibration. The peak at 783 cm^{-1} is due to O-Si-O symmetric stretching. The peak at 553.5 cm^{-1} is due to octahedral linkage of Si-O-Al. In Fig. 3c, the spectra of wheat bran are shown. The peaks at 3511.7 cm^{-1} and 3263 cm^{-1} are due to -OH stretching and NH stretching, respectively. The -OH groups in question may be from adsorbed water, primary and alcohol groups in cellulose and hemicelluloses in bran. The peak at 2926.5 cm^{-1} is due to CH stretching of methylene group in polysaccharides in bran [38]. The peak at 2400 cm^{-1} is because of CO_2 in air, the medium in which the IR spectra were taken.

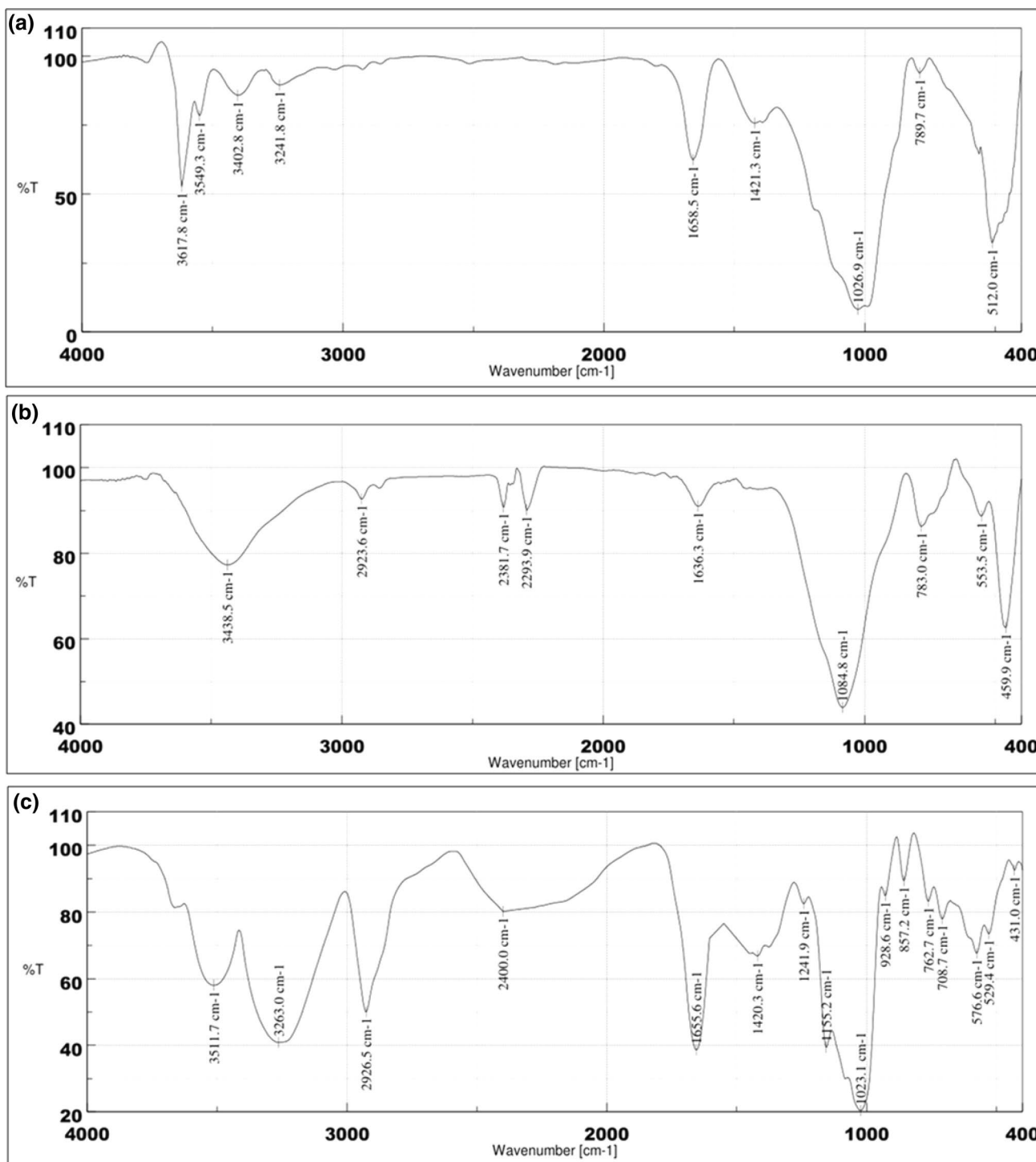


Fig. 3 **a** FTIR spectra of sodium-activated calcium bentonite, **b** FTIR spectra of fly ash, **c** FTIR spectra of wheat bran

The band at 1655.6 cm⁻¹ is due to conjugated C=O bond stretching. The peaks at 857.5 and 1420 cm⁻¹ indicate the presence of CH₂ groups. The peak at 1155.2 cm⁻¹ is due to aromatic -OH bond, while the peak at 1241.9 cm⁻¹ is associated with CH₂OH group present in carbohydrates [39], as well as the C-O-H deformation. The peak

at 1023 cm⁻¹ could be because C-O-C group in raw bran [40]. The peak at 928.6 cm⁻¹ is due to out-of-plane blending of C-H in cyclohexane [41]. The peak at 762.7 is because of -C-H deformation. The band at 708.7 cm⁻¹ is probably because of =C-H bending. The peaks at 529.4 and 576.6 cm⁻¹ are probably because of cyclic C-H

out-of-plane deformation. The weak band observed at 431 cm^{-1} is probably due to Fe–O or Si–O bends [42]. The BET surface areas of sodium-activated calcium bentonite, fly ash and wheat bran were $95.4\text{ m}^2/\text{g}$, $0.4\text{ m}^2/\text{g}$ and $0.3\text{ m}^2/\text{g}$, respectively.

3.4 Process standardization

3.4.1 Effect of contact time

The effect of contact time on the adsorption of Fe(II), Ni(II) and Cu(II) ions from the multi-component solution was studied at various intervals between 1 and 120 min (Table 3). The results are summarized in Fig. 4a, and it is clear that the trend is similar for all three ions. It is evident that equilibrium is reached after 90 min for all three ions, which is relatively fast. The adsorption is fast initially and becomes slower (after 35 min) as it attains equilibrium. This can be explained by the availability of fresh/vacant binding sites and external surface area of adsorbent during initial stages, which get exhausted as adsorption proceeds [43]. The free ions in metal solution may also experience some repulsion with adsorbed ions which

reduces further adsorption [37]. The percent removal values at equilibrium ($t = 120\text{ min}$) for metals ions Fe(II), Ni(II) and Cu(II) were found to be 96.93, 74.64 and 70.89, respectively. It has to be noted that segregation of adsorbents due to density differences was not observed in the adsorption vessel. This is attributed to the presence of the magnetic stirrer which improves mixing.

3.4.2 Effect of pH

The pH of aqueous solution is known to be an important variable as it controls the uptake of metal ions at the water–sorbent interface. It directly influences the adsorption capacity and needs to be carefully optimized [18]. For investigating the same, pH was varied between 2 and 7 (Table 3) and %R values were noted. It was observed that the percent removal increased with increasing pH for all three ions, as seen in Fig. 4b. At low pH, the lower percent removal is due to excess H^+ ions surrounding the binding sites and making them positively charged by protonation reaction [31]. This leads to repulsion of the metal ions from the adsorbent which makes adsorption unfavorable. The hydrogen ions also offer competition to the metal ions in

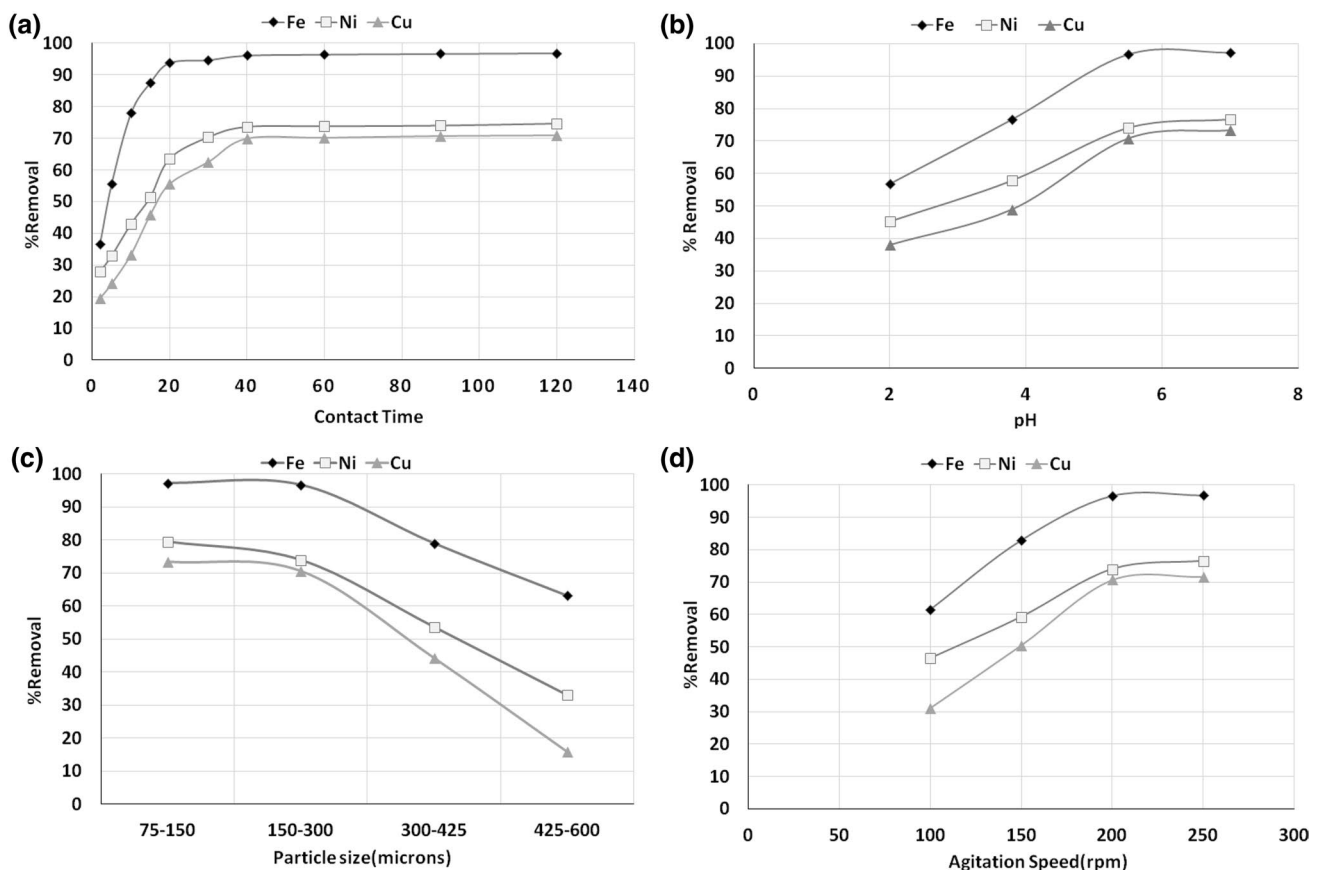


Fig. 4 **a** Effect of contact time required for percent removal of metal ions, **b** effect of pH on percent removal of metal ions, **c** effect of particle size on percent removal of metal ions, **d** effect of agitation speed on percent removal of metal ions

the solution [14]. At high pH, the presence of OH⁻ favors deprotonation reaction which reduces the positive charge density on the adsorbent, favoring adsorption of metal ions [30, 37]. For pH > 7, the metal ions in the effluent precipitated due to the formation of hydroxides [14], so investigation for basic range of pH was not done. For all other investigations, a pH of 5.5 was chosen as optimum as it gave higher %R value and was safely in the acidic region where precipitation of metal hydroxides does not happen.

3.4.3 Effect of particle size

Batch adsorption experiments with adsorbent in size ranges of 600–425, 425–300, 300–150, 150–75 μ (Table 3) were used to investigate the effect of particle size. The adsorbent blend was made by taking required weight fractions from appropriate size ranges of each adsorbent. It can be seen from Fig. 4c that the percent removal increases with decreasing particle size. This is because smaller particles have a larger specific surface area, which provide larger number of active sites for the metal ions to bind onto. A particle size of 150–300 μ was chosen as optimum for use in all experiments.

3.4.4 Effect of agitation speed

Agitation of the liquid phase is an important parameter in adsorption phenomena as it influences the mass transfer of metal ions from bulk liquid to surface of the adsorbent. To study the effect of the same, batch adsorption experiments were performed (Table 3) at four different speeds of 100 rpm, 150 rpm, 200 rpm and 250 rpm. Results depicted in Fig. 4d show that as the agitation speed was increased, the % removal of metal ions also increased. This trend was similar for all three ions studied. This is because with the increase in agitation speed the turbulence in liquid phase increases, which increases the external mass transfer coefficients and reduces the boundary layer effect [44]. This leads to faster adsorption as the external resistance decreases. At 200 rpm, the percent removal was Fe(II)(96.7%) > Ni(II)(74%) > Cu(II) (70.7%). Increasing the agitation speed above 200 rpm did not lead to a significant increase in % removal, so this was chosen as the optimum value for all other experiments.

3.4.5 Effect of adsorbent dosage

The effect of adsorbent dosage was investigated by varying the dose between 0.2 and 1 g/50 ml (Table 3). The results are summarized in Fig. 5a, b. The percent removal increased with the increase in adsorbent dosage for all three ions. This is because at low dosages, the active sites available to the ions were limited, but with more dosage there is more area, and more active sites for the ions

to bind to, which increases adsorption percentage. But the adsorption capacity decreased with the increase in dosage Fig. 5b. This is due to two reasons: (1) Increased adsorbent quantity decreases the saturation of active sites. This causes the number of covered sites per unit mass of adsorbent to fall, which leads to a fall in capacity, and (2) increase in concentration of adsorbent in solution causes particle agglomeration which reduces the specific surface area and increases diffusion path length, both of which affect adsorption capacity negatively [45].

3.4.6 Effect of temperature

The effect of temperature on adsorption onto the adsorbent blend was investigated at four different temperatures of 20 °C, 30 °C, 40 °C and 50 °C (Table 3). It can be seen from Fig. 5c that the percent removal of Fe(II) and Cu(II) increased with the increase in temperature, indicating that their adsorption onto adsorbents is endothermic [46, 47]. For Ni(II) however, the percent removal decreased, indicating exothermic adsorption of Ni(II) [37].

3.4.7 Adsorption kinetic models

For the kinetic study, batch experiments were conducted with conditions: contact time 2–120 min at 30 °C, 1 g/50 mL dosage of adsorbent, pH of 5.5, agitation speed 200 rpm and particle size of 150–300 μ. To identify the suitable kinetic model, kinetic data for the adsorption of Fe(II), Ni(II) and Cu(II) ions were analyzed by pseudo-first-order (Eq. 4) and pseudo-second-order (Eq. 5) models where q_e is the adsorption capacity at equilibrium, q_t is the adsorption capacity at any time t , k_1 is the rate constant for pseudo-first-order kinetics (min⁻¹) and k_2 is the rate constant of pseudo-second-order kinetics (g/mg min).

$$\ln(q_e - q_t) = \ln q_e - k_1 t \quad (4)$$

$$\frac{t}{q_t} = \frac{1}{k_2 q_e^2} + \frac{t}{q_e} \quad (5)$$

It was found that pseudo-first-order model (plots not shown here) did not fit well for the three metal ions. Pseudo-second-order model [15, 48] on the other hand showed good linearity as shown in Fig. 6a. The parameters for the pseudo-second-order model are listed in Table 5. The equilibrium adsorption capacity (q_e) values decreased as Fe(II) > Ni(II) > Cu(II). The experimentally calculated q_e and the theoretical q_e value were very close to each other. This fact, together with $R^2 > 0.99$, helps us conclude that the pseudo-second-order model describes the system well for all three ions.

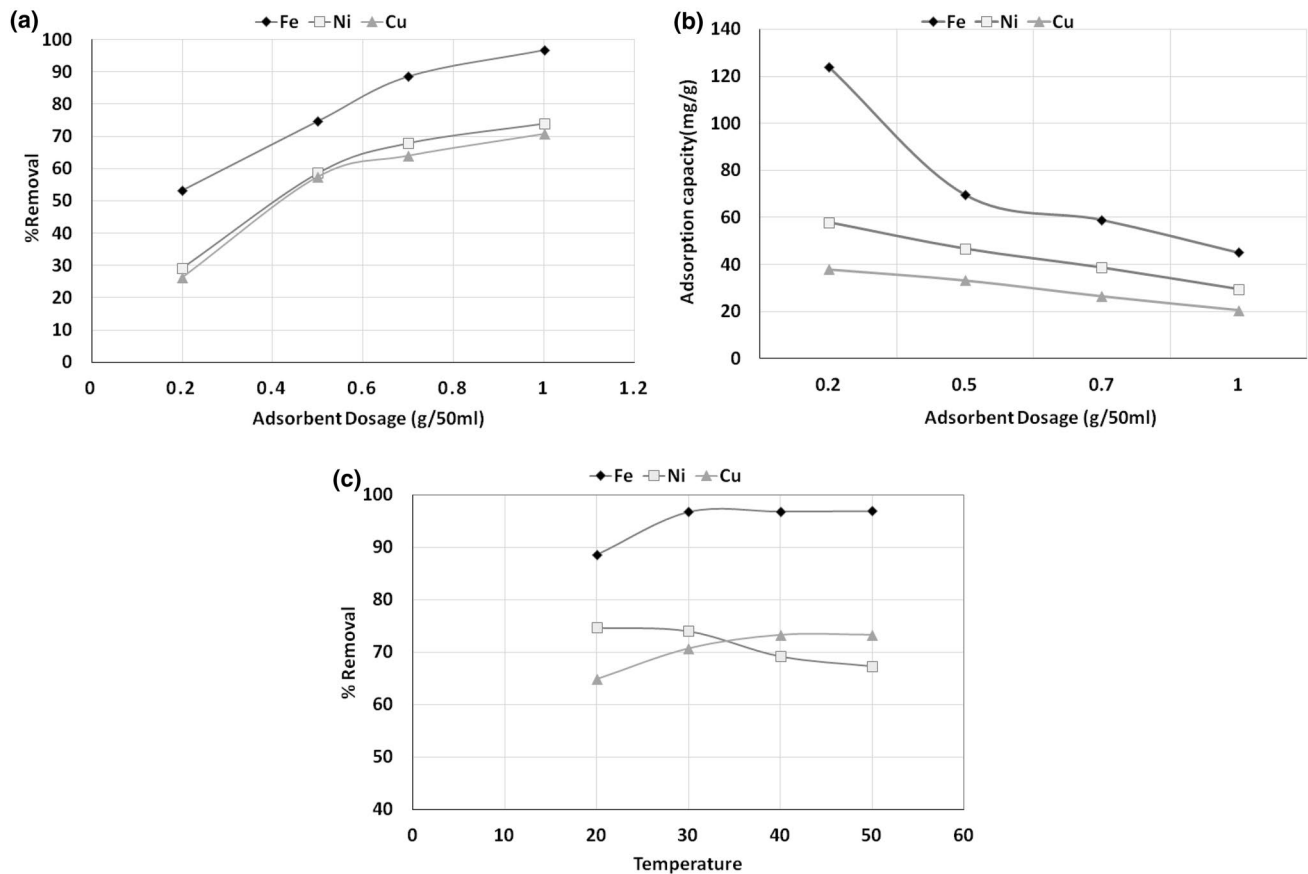


Fig. 5 **a** Effect of adsorbent dosage on percent removal of metal ions, **b** the effect of adsorbent dosage on adsorption capacity (q_e), **c** the effect of temperature on percent removal of metal ions

3.4.8 Intraparticle diffusion model

The pseudo-second-order kinetic model describes the overall adsorption kinetics satisfactorily, but it gives no information about the rate controlling steps. Adsorption of heavy metal ions onto porous sorbent particles can be described by four consecutive transport steps: (1) transport of ions in the bulk solution; (2) diffusion across the boundary layer around the sorbent particles; (3) diffusion of ions within the pores of the sorbent particles, i.e., intraparticle diffusion; and (4) adsorption of ions on the solid particle surface [49]. In porous adsorbents, intraparticle diffusion is known to play a prominent role, so to investigate the same, kinetic data were analyzed with Weber and Morris intraparticle diffusion model [48, 50]. According to this model, the adsorption capacity (q_t) is related to time (t) as shown in Eq. 6, where k_{id} is the intraparticle diffusion rate constant ($\text{mg g}^{-1} \cdot \text{min}^{-0.5}$) and intercept C is dependent on the effect of diffusion across the liquid boundary layer. Larger the value of C , greater the effect of boundary layer diffusion.

$$q_t = k_{id} \cdot t^{0.5} + C \quad (6)$$

When intraparticle diffusion is the sole rate controlling step, Eq. 6 yields a straight line passing through the origin. A deviation from the origin, quantified by the intercept C , indicates some level of control by boundary layer diffusion. Plots of q_t versus $t^{0.5}$ for the three metal ions are shown in Fig. 6b. It is apparent that the plot exhibits multi-linearity with three distinct linear regions of different slopes for all three metals. This indicates that in different time intervals, different steps are controlling the overall rate of adsorption. The initial region has the highest slope which is ascribed to the fast adsorption of metal ions onto the exterior surface of fresh adsorbent particles, as it would face only the boundary layer diffusion as rate-limiting step. The second region has a lower slope, i.e., adsorption happens more slowly. This region describes the adsorption rates after all the external sites have been saturated. Now the metal ions have to diffuse through the intraparticle pores to adsorb onto the pore surface area of the particles, and intraparticle diffusion has become the rate-limiting step. This is considerably slower as compared to the first region where boundary layer diffusion (in an agitated liquid) was the rate-limiting step, hence the lower

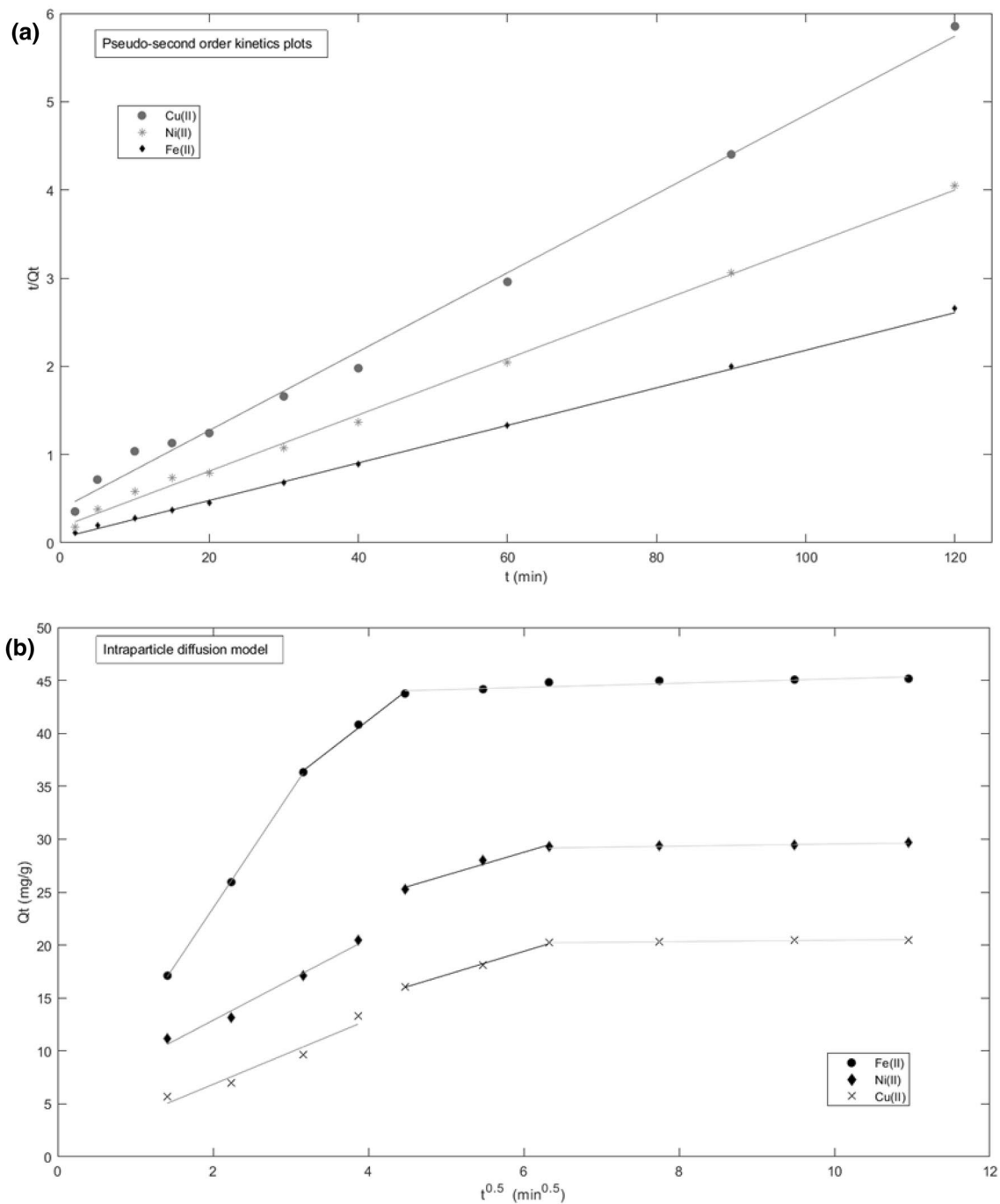


Fig. 6 **a** Pseudo-second-order kinetics plots for Fe(II), Ni(II) and Cu(II) ions, **b** intraparticle diffusion model plots, adsorption capacity versus $t^{0.5}$ for Fe(II), Ni(II) and Cu(II)

slope. In the third region, the adsorption happens at a very low rate, quantified by the almost zero slopes. This is the phase after which almost all the active sites have become saturated and the system has reached equilibrium. Similar multi-linear behavior was reported by other authors [51]. The k_{id} and C values calculated from each linear region for each metal ion, and the corresponding R^2 values are

summarized in Table 6. As is to be expected, the k_{id} values followed the order $k_{id1} > k_{id2} > k_{id3}$ for all the metal ions. The multi-linearity of the plot implies that intraparticle diffusion is not the sole rate controlling step for adsorption of the metal ions on the adsorbents in the blend, but it is one of the rate-limiting steps along with boundary layer diffusion.

Table 5 Pseudo-second-order kinetic parameters for all three metal ions

Metal	C_o (mg/L)	K_2 (g/mg.min)	q_e (calculated) (mg/g)	q_e (experiment) (mg/g)	R^2
Fe(II)	931.8	0.00849	46.97	45.07	0.9989
Ni(II)	795.2	0.00582	31.377	29.44	0.9972
Cu(II)	578.3	0.00527	22.37	20.445	0.9943

3.4.9 Adsorption isotherm

The experimental equilibrium data were collected at conditions with different adsorbent dosages of 0.2, 0.5, 0.7, 1 g per 50 mL of effluent with condition of 5.5 pH, temperature 303 K, agitation speed 200 rpm, particle size 150–300 μ and 90 min' contact time. These data for the adsorption of Fe(II), Ni(II) and Cu(II) were analyzed with two equilibrium models: Langmuir and Freundlich adsorption isotherms. In linear forms, the Langmuir and Freundlich isotherms are represented by Eqs. 7 and 8, respectively, where q_e is the amount of metal adsorbed at equilibrium (mg/g), b is the Langmuir constant related to affinity between adsorbate and adsorbent (L/mg), q_m is the maximum adsorption capacity (mg/g), C_e is the concentration of metal ions at equilibrium (mg/L) and K_f and n are Freundlich constants and represent adsorption capacity and adsorption intensity, respectively. Langmuir model Eq. (7) assumes that there are a finite number of binding sites on the adsorbent which are homogeneously distributed over its surface and only a single monolayer is formed and there was no interaction between the adsorbed molecules. Once the adsorbent was covered with monolayer, the solute transport does not influence the sorption. Adsorption efficiency can be predicted by a dimensionless constant separation factor or equilibrium parameter R_L Eq. (9) where C_o is the initial metal concentration (mg/L) and b is the Langmuir constant (L/mg). If $R_L > 1$, then the adsorption is unfavorable; if $R_L = 1$, then the adsorption is linear; if $0 < R_L < 1$, then the adsorption is favorable; and if $R_L = 0$, it is irreversible [11].

$$\frac{C_e}{q_e} = \frac{1}{q_m b} + \frac{C_e}{q_m} \tag{7}$$

$$\log q_e = \log K_f + \frac{1}{n} \log C_e \tag{8}$$

Table 6 Intraparticle diffusion model constants for adsorption metal ions onto adsorbent blend

Metal	C_o	k_{id1}	C_1	R_1^2	k_{id2}	C_2	R_2^2	k_{id3}	C_3	R_3^2
Fe(II)	931.8	11	1.4832	1	5.685	18.495	0.995	0.2026	43.115	0.776
Ni(II)	795.2	3.8491	5.1888	0.982	2.1646	15.774	0.978	0.10279	28.521	0.907
Cu(II)	578.3	3.0483	0.74183	0.948	2.2246	6.0556	0.995	0.065298	19.798	0.976

C_o in mg L⁻¹, k_{id} values in mg g⁻¹.min^{-0.5}

$$R_L = \frac{1}{1 + bC_o} \tag{9}$$

Freundlich isotherm Eq. (8) is an exponential equation which states that the adsorbate concentration on surface of the adsorbent increases as the adsorbate concentration in the solution increases. Freundlich isotherm is an empirical equation which is used for heterogeneous systems. For testing the applicability of these models, linear plots of $\frac{C_e}{q_e}$ versus C_e and $\log(q_e)$ versus $\log C_e$ were made. They are shown in Fig. 7a, b, respectively. The R^2 values indicated that Freundlich isotherm fit the experimental data somewhat better compared to the Langmuir model. The parameters associated with the two models are tabulated in Table 7. For the Freundlich model, the values of K_f (order) indicate that the preferential order of adsorption follows Fe(II) > Ni (II) > Cu(II). The values of n are greater than 1 for Fe(II), Ni(II) and Cu(II) which indicate favorable adsorption onto the blend [48]. From the Langmuir isotherm model, the q_m values are in the order Fe(II) 146.1 mg/g > Ni(II) 115.9 mg/g > Cu(II) 74.5 mg/g which are quite high. The high maximum adsorption capacity values prove the effectiveness of blending different adsorbents in treating waste water. The R_L values for all three metal ions lie between 0 and 1, which imply favorable adsorption [14, 15, 48]. It was observed that neither Langmuir nor Freundlich isotherm fit the model perfectly. This is because the adsorbent (blend) being used is heterogeneous, and each adsorbent-metal system follows a different adsorption isotherm, so the net effect cannot be explained by a single Langmuir or Freundlich model [52, 53].

3.4.10 Thermodynamics of adsorption

The thermodynamic parameter Gibbs free energy change (ΔG°) can be calculated by Eq. 10

$$\Delta G^\circ = -RT \ln K_d \tag{10}$$

$$K_d = \frac{q_e}{C_e} \tag{11}$$

where T is the absolute temperature in K, R is the universal gas constant (8.314 J/mol K) and K_d is the thermodynamic distribution coefficient calculated by Eq. 11. K_d values

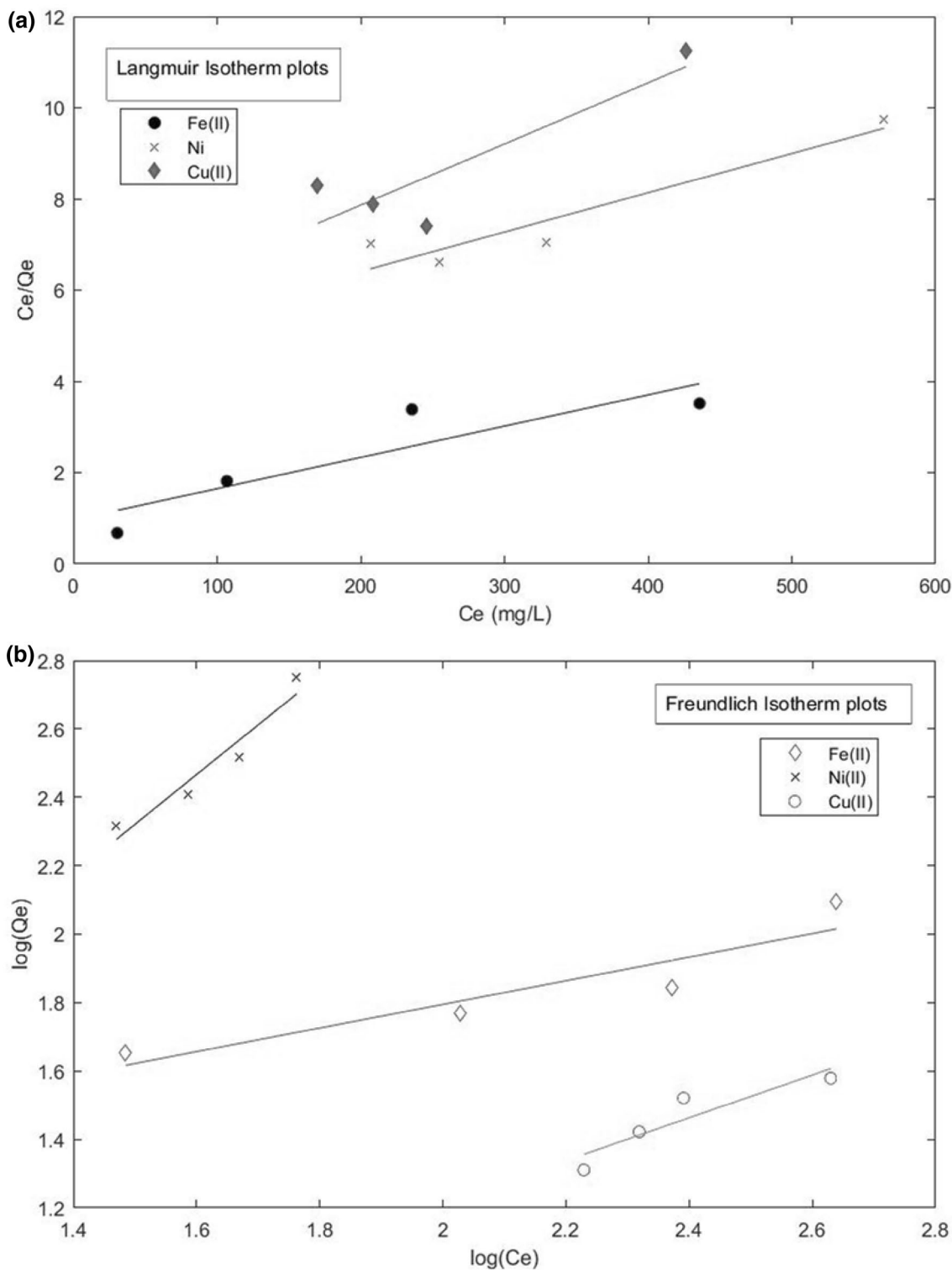


Fig. 7 **a** Langmuir isotherm plots for adsorption experiments for Fe(II), Ni(II) and Cu(II) ions and **b** Freundlich plots for the adsorption experiments for Fe(II), Ni(II) and Cu(II) ions

were calculated by the equilibrium values of q_e and C_e at different temperatures (293 K, 303 K, 313 K and 323 K) while all other parameters were constant (1 g per 50 mL

of effluent maintained at 5.5 pH, temperature 303 K, agitation speed 200 rpm, particle size 150–300 μ and 90 min' contact time). ΔG° values were calculated using Eq. 10 at

Table 7 Langmuir and Freundlich isotherm constants

Metal	Langmuir isotherm				Freundlich isotherm		
	q_m (mg/g)	b (L/mg)	R^2	R_L	K_F (mg/g)	n	R^2
Fe(II)	146.1155	0.0071	0.801	0.131	3.0198	2.8997	0.854
Ni(II)	115.9541	0.0018	0.898	0.411	1.0325	1.5711	0.925
Cu(II)	74.5045	0.0026	0.779	0.400	0.96118	1.5970	0.831

Table 8 Thermodynamic parameters for Fe(II), Ni(II) and Cu(II) ions

Metal	Temperature (K)	K_d (mg/L)	ΔG° (KJ/mol)
Fe	293	0.3874	2.309
	303	1.4823	-0.991
	313	1.5238	-1.096
	323	1.5618	-1.197
Ni	293	0.1475	4.662
	303	0.1424	4.909
	313	0.1122	5.692
	323	0.1027	6.110
Cu	293	0.092	5.809
	303	0.120	5.326
	313	0.1375	5.165
	323	0.1375	5.328

different temperatures. The calculated values are listed in Table 8. The negative value of ΔG° for Fe(II) at 303 K, 313 K and 323 K shows that the adsorption process is feasible and spontaneous at these temperatures [18], but at 293 K the ΔG° value was positive indicating non-spontaneous adsorption. For Ni(II) and Cu(II), the ΔG° values were found to be positive at all temperatures investigated, indicating non-spontaneous adsorption. For Fe(II), the free energy decreased (became more negative) with increasing temperature, i.e., adsorption became more spontaneous. For Ni(II), the free energy became more positive with increasing temperature, indicating decreasing spontaneity with increasing temperature. For Cu(II), the spontaneity increased with increasing temperature.

4 Conclusion

In the present study, the metal ions of Fe(II), Cu (II) and Ni(II) besides many others like Zn(II), As(II), Cd(II) were removed from an industrial effluent using various adsorbents from industrial and agricultural wastes. After the initial screening of the candidates, three best ones in terms of percent metal removal, viz. calcium bentonite, wheat bran and fly ash, were selected, and then, their possible blends were tried that could give the maximum metal removal under similar conditions. These three adsorbents were characterized with FTIR for identifying the functional groups and BET analysis to measure their

specific surface areas. The best adsorbent composition which gave maximum metal removal for the effluent was 60–20–20 wt% of calcium bentonite–fly ash–wheat bran. Various process parameters, viz. contact time, pH, sorbent dosage, agitation speed and particle size, were found to affect the adsorption of metals Fe(II), Cu(II) and Ni(II) onto the adsorbent blend. These parameters were standardized rigorously to have the highest possible metal removal. The optimal set of conditions identified were pH, 5–7; contact time, 60–90 min; agitation speed of 200 rpm; adsorbent dosage of 1 g/50 mL; and particle size of 150–300 μ . Kinetic studies were done at the optimal conditions to estimate the kinetic parameters, using pseudo-first- and pseudo-second-order models. It was found that pseudo-second-order model could fit the data better than the pseudo-first-order model for all three metal ions. The kinetic constants were found to be 8.49×10^{-3} , 5.82×10^{-3} , $5.27 \times 10^{-3} \frac{\text{g}}{\text{mg min}}$ for Fe(II), Ni(II) and Cu(II), respectively. Weber and Morris intraparticle diffusion model was used to analyze the kinetic data, and it was found that there are multiple rate-limiting steps during the adsorption process, including intraparticle diffusion. The equilibrium data were analyzed using Langmuir and Freundlich isotherm models. The maximum Langmuir adsorption capacity values of the three metals for the adsorbent blend were Fe(II) 146.1 mg/g > Ni (II) 115.9 mg/g > Cu (II) 74.5 mg/g. It was observed that neither Langmuir nor Freundlich models fit the experimental data satisfactorily. This is observed because the adsorbent used was heterogeneous (blend of three adsorbents), and each component shows different isotherm behaviors. The thermodynamic feasibility and spontaneity of the adsorption process were studied by estimating the Gibbs free energy for each metal ion. For Ni (II) and Cu (II), the adsorption was found to be non-spontaneous at all temperatures studied. For Fe(II), the adsorption was spontaneous at all temperatures studied, except at 293 K. This work demonstrated the successful use of adsorbent blends to treat wastewater containing multiple heavy metals.

Acknowledgements The authors wish to thank HBL Power Systems Ltd., Hyderabad, for providing the effluent needed for our experimental studies. We also thank Ms. Megha Gupta for her contribution in this work.

Compliance with ethical standards

Conflict of interest We, the authors declare that there is no conflict of interest in this work.

References

- Ghorai S, Sarkar AK, Pal S (2014) Rapid adsorptive removal of toxic Pb²⁺ ion from aqueous solution using recyclable, biodegradable nanocomposite derived from templated partially hydrolyzed xanthan gum and nanosilica. *Bioresour Technol* 170:578–582. <https://doi.org/10.1016/j.biortech.2014.08.010>
- Sousa FW, Oliveira AG, Ribeiro JP, Rosa MF, Keukeleire D, Nascimento RF (2010) Green coconut shells applied as adsorbent for removal of toxic metal ions using fixed-bed column technology. *J Environ Manag* 91:1634–1640. <https://doi.org/10.1016/j.jenvman.2010.02.011>
- Tunali S, Çabuk A, Akar T (2006) Removal of lead and copper ions from aqueous solutions by bacterial strain isolated from soil. *Chem Eng J* 115:203–211. <https://doi.org/10.1016/j.cej.2005.09.023>
- Wang LK, Vaccari DA, Li Y, Shammas NK (2005) Chemical precipitation. In: Wang LK, Hung Y-T, Shammas NK (eds) *Physicochemical treatment processes*. Humana Press, Totowa, pp 141–197. <https://doi.org/10.1385/1-59259-820-x:141>
- Juang RS, Shiau RC (2000) Metal removal from aqueous solutions using chitosan-enhanced membrane filtration. *J Membr Sci* 165:159–167. [https://doi.org/10.1016/S0376-7388\(99\)00235-5](https://doi.org/10.1016/S0376-7388(99)00235-5)
- Tzanetakis N, Taama WM, Scott K, Jachuck RJJ, Slade RS, Varcoe J (2003) Comparative performance of ion exchange membranes for electrodialysis of nickel and cobalt. *Sep Purif Technol* 30:113–127. [https://doi.org/10.1016/S1383-5866\(02\)00139-9](https://doi.org/10.1016/S1383-5866(02)00139-9)
- Barakat MA, Chen YT, Huang CP (2004) Removal of toxic cyanide and Cu(II) ions from water by illuminated TiO₂ catalyst. *Appl Catal B* 53:13–20. <https://doi.org/10.1016/j.apcatb.2004.05.003>
- Al-Qodah Z, Al-Shannag M (2017) Heavy metal ions removal from wastewater using electrocoagulation processes: a comprehensive review. *Sep Sci Technol (Phila)* 52:2649–2676. <https://doi.org/10.1080/01496395.2017.1373677>
- Barakat MA (2011) New trends in removing heavy metals from industrial wastewater. *Arab J Chem* 4:361–377. <https://doi.org/10.1016/j.arabj.2010.07.019>
- Naushad M, Ahamad T, AlOthman ZA, Al-Muhtaseb AH (2019) Green and eco-friendly nanocomposite for the removal of toxic Hg(II) metal ion from aqueous environment: adsorption kinetics & isotherm modelling. *J Mol Liq* 279:1–8. <https://doi.org/10.1016/j.molliq.2019.01.090>
- Kumar P, Kumar P (2019) Removal of cadmium (Cd-II) from aqueous solution using gas industry-based adsorbent. *SN Appl Sci* 1:1–8. <https://doi.org/10.1007/s42452-019-0377-8>
- AL-Othman ZA, Ali R, Naushad M (2012) Hexavalent chromium removal from aqueous medium by activated carbon prepared from peanut shell: adsorption kinetics, equilibrium and thermodynamic studies. *Chem Eng J* 184:238–247. <https://doi.org/10.1016/j.cej.2012.01.048>
- Naushad M, Vasudevan S, Sharma G, Kumar A, AlOthman ZA (2016) Adsorption kinetics, isotherms, and thermodynamic studies for Hg²⁺ adsorption from aqueous medium using alizarin red-S-loaded amberlite IRA-400 resin. *Desalin Water Treat* 57:18551–18559. <https://doi.org/10.1080/19443994.2015.1090914>
- Naushad M, Ahamad T, Sharma G, Al-Muhtaseb AH, Albadarin AB, Alam MM, AlOthman ZA, Alshehri SM, Ghfar AA (2016) Synthesis and characterization of a new starch/SnO₂ nanocomposite for efficient adsorption of toxic Hg²⁺ metal ion. *Chem Eng J* 300:306–316. <https://doi.org/10.1016/j.cej.2016.04.084>
- Alqadami AA, Naushad M, Abdalla MA, Ahamad T, AlOthman ZA, Alshehri SM, Ghfar AA (2017) Efficient removal of toxic metal ions from wastewater using a recyclable nanocomposite: a study of adsorption parameters and interaction mechanism. *J Clean Prod* 156:426–436. <https://doi.org/10.1016/j.jclepro.2017.04.085>
- Alqadami AA, Naushad M, AlOthman ZA, Ghfar AA (2017) Novel metal-organic framework (MOF) based composite material for the sequestration of U(VI) and Th(IV) metal ions from aqueous environment. *ACS Appl Mater Interfaces* 9:36026–36037. <https://doi.org/10.1021/acsami.7b10768>
- Alqadami AA, Naushad M, AlOthman ZA, Ahamad T (2018) Adsorptive performance of MOF nanocomposite for methylene blue and malachite green dyes: kinetics, isotherm and mechanism. *J Environ Manag* 223:29–36. <https://doi.org/10.1016/j.jenvman.2018.05.090>
- Naushad M, Ahamad T, Al-Maswari BM, Alqadami AA, Alshehri SM (2017) Nickel ferrite bearing nitrogen-doped mesoporous carbon as efficient adsorbent for the removal of highly toxic metal ion from aqueous medium. *Chem Eng J* 330:1351–1360. <https://doi.org/10.1016/j.cej.2017.08.079>
- Naushad M (2014) Surfactant assisted nano-composite cation exchanger: development, characterization and applications for the removal of toxic Pb²⁺ from aqueous medium. *Chem Eng J* 235:100–108. <https://doi.org/10.1016/j.cej.2013.09.013>
- Gupta VK, Srivastava SK, Mohan D, Sharma S (1998) Design parameters for fixed bed reactors of activated carbon developed from fertilizer waste for the removal of some heavy metal ions. *Waste Manag* 17:517–522. [https://doi.org/10.1016/S0956-053X\(97\)10062-9](https://doi.org/10.1016/S0956-053X(97)10062-9)
- Horsfall M, Abia AA, Spiff AI (2006) Kinetic studies on the adsorption of Cd²⁺, Cu²⁺ and Zn²⁺ ions from aqueous solutions by cassava (*Manihot sculenta* Cranz) tuber bark waste. *Bioresour Technol* 97:283–291. <https://doi.org/10.1016/j.biortech.2005.02.016>
- Wang XS, Li ZZ, Tao SR (2009) Removal of chromium (VI) from aqueous solution using walnut hull. *J Environ Manag* 90:721–729. <https://doi.org/10.1016/j.jenvman.2008.01.011>
- Zouboulis AI, Loukidou MX, Matis KA (2004) Biosorption of toxic metals from aqueous solutions by bacteria strains isolated from metal-polluted soils. *Process Biochem* 39:909–916. [https://doi.org/10.1016/S0032-9592\(03\)00200-0](https://doi.org/10.1016/S0032-9592(03)00200-0)
- Jianlong W (2002) Biosorption of copper(II) by chemically modified biomass of *Saccharomyces cerevisiae*. *Process Biochem* 37:847–850. [https://doi.org/10.1016/S0032-9592\(01\)00284-9](https://doi.org/10.1016/S0032-9592(01)00284-9)
- Chojnacka K, Chojnacki A, Górecka H (2004) Trace element removal by *Spirulina* sp. from copper smelter and refinery effluents. *Hydrometallurgy* 73:147–153. <https://doi.org/10.1016/j.hydromet.2003.10.003>
- Amarasinghe BMWPK, Williams RA (2007) Tea waste as a low cost adsorbent for the removal of Cu and Pb from wastewater. *Chem Eng J* 132:299–309. <https://doi.org/10.1016/j.cej.2007.01.016>
- Singh KK, Rastogi R, Hasan SH (2005) Removal of Cr(VI) from wastewater using rice bran. *J Colloid Interface Sci* 290:61–68. <https://doi.org/10.1016/j.jcis.2005.04.011>
- Arunlertaree C, Kaewsomboon W, Kumsopa A, Pokethitiyook P, Panyawathanakit P (2007) Removal of lead from battery manufacturing wastewater by egg shell. *Songklanakarin J Sci Technol* 29:857–868. <https://doi.org/10.1016/j.proenv.2012.01.372>
- Oubagaranadin JUK, Sathyamurthy N, Murthy ZVP (2007) Evaluation of Fuller's earth for the adsorption of mercury from aqueous solutions: a comparative study with activated carbon. *J Hazard Mater* 142:165–174. <https://doi.org/10.1016/j.jhazmat.2006.08.001>

